Activation of the TP53 pathway is a therapeutic vulnerability in NUP98::KDM5A^{+} pediatric AML

Luca Nunzio Cifarelli[1,2], Hasan Issa[2], Ludovica Proietti[6], Konstantin Schuschel[2], Lucie Gack[3], Katja Menge[3], Christian Ihling[4,5], Meike Vogler[1], Andrea Sinz[4,5], Jan-Henning Klusmann[2*], Dirk Heckl[1,2*]

[1] Institute for Experimental Pediatric Hematology and Oncology, Goethe-University Frankfurt, Frankfurt am Main, Germany

[2] Dep. of Pediatrics, Goethe-University Frankfurt, Frankfurt am Main, Germany

[3] Dep. of Pediatric Hematology and Oncology, Martin-Luther-University Halle-Wittenberg, Halle, Germany

[4] Dep. of Pharmaceutical Chemistry and Bioanalytics, Martin-Luther-University Halle-Wittenberg, Halle, Germany

[5] Center for Structural Mass Spectrometry, Martin-Luther-University Halle-Wittenberg, Halle, Germany

[6] Centre of Biological Sciences, University of Veterinary Medicine, Vienna, Austria

*authors contributed equally to the work

Correspondence: Dirk Heckl, Institute for Experimental Pediatric Hematology and Oncology, Goethe-University Frankfurt, Komturstraße 3a, 60528 Frankfurt am Main, Germany; e-mail: heckl@med.uni-frankfurt.de.

Disclosures: J-HK has advisory roles for Boehringer, Roche and Jazz Pharmaceuticals. All other authors declare that the manuscript was written in the absence of any commercial or financial relationships that could be perceived as a potential conflict of interest.

27 # Graphical abstract

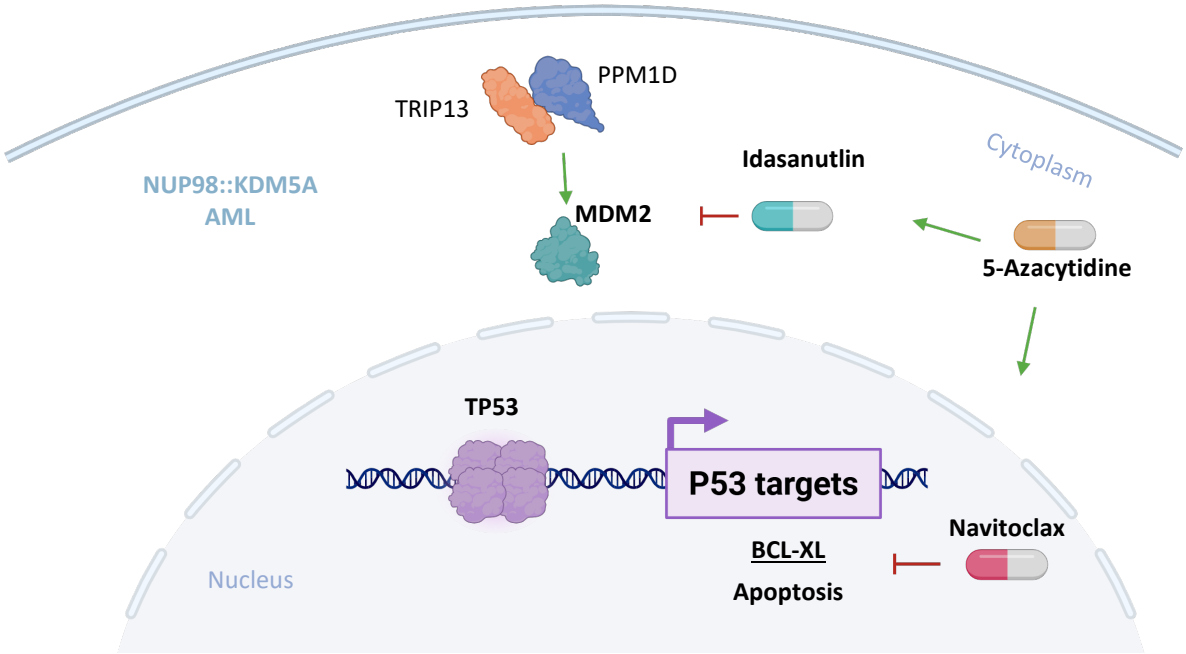

28

29 # Abstract

30 Pediatric acute myeloid leukemia (AML) driven by the NUP98::KDM5A fusion is an
31 aggressive subtype predominantly arising in infancy, with limited therapeutic options
32 and poor prognosis. Using matched fetal and adult hematopoietic stem and progenitor
33 cell models, we demonstrate that NUP98::KDM5A-driven leukemia originating in a fetal
34 context exhibits enhanced aggressiveness and sustains fetal-specific transcriptional
35 programs. Functional genomic and proteomic analyses identified a critical dependency
36 on the AAA^{+} ATPase TRIP13, which binds the phosphatase PPM1D to suppress TP53
37 activation. Pharmacologic inhibition of TRIP13 or combined treatment with idasanutlin,
38 navitoclax, and 5-azacytidine effectively reactivated TP53 signaling and induced
39 apoptosis in a synergistic manner in NUP98::KDM5A AML models. These findings
40 reveal a developmentally regulated TRIP13/PPM1D–TP53 survival axis that can be

41 exploited for targeted therapy, offering a mechanistically grounded and translatable
42 strategy to improve outcomes for this high-risk pediatric leukemia patients.

43 Introduction

44 Pediatric acute myeloid leukemia (AML) is a heterogenous disease, accounting for
45 ~15-20% of all pediatric acute leukemias, and its mutational landscape substantially
46 differs from that of adult AML even within different pediatric age groups [1-5]. The
47 different subgroups and the distinct mutations occurring in pediatric AML may in part
48 be attributable to the ontogeny and the cellular environment, which is particularly
49 prominent in infant AML (≤2 years of age) [6-8]. Indeed, in some instances, oncogenic
50 driver mutations have been detected at birth pointing to an *in utero* origin of the disease
51 that is linked with fetal hematopoiesis [9, 10]. While definitive proof is still missing, an
52 association of the molecular properties of fetal cells and their environment may explain
53 the high prevalence of certain chromosomal translocations and subgroups.
54 One of these highly prevalent subgroups is acute megakaryoblastic leukemia (AMKL),
55 which is an aggressive form of AML associated with lower event-free and overall
56 survival in the absence of underlying Down syndrome (trisomy 21) and occurs in up to
57 15% of AML children [11-13].
58 A main genetic driver event in AMKL is the chromosomal translocation t(11;12), which
59 generates the NUP98::KDM5A fusion oncoprotein composed of the N-terminal glycine-
60 leucine-phenylalanine-glycine (GLFG) repeat motif of NUP98 and the C-terminal plant
61 homeodomain finger (PHD3) of histone lysine demethylase KDM5A (also known as
62 JARID1A) [14, 15].
63 Several studies have shown that *NUP98::KDM5A* drives transformation of murine
64 hematopoietic stem and progenitors cells (HSPCs) and recapitulates the principal
65 aspect of the disease, such as the transcriptional upregulation of *HOXA* and *HOXB*

66 gene clusters [16-18]. However, in contrast to *CBFA2T3::GLIS2* or *KMT2A*-rearranged
67 AML [6], the impact and the molecular role of the fetal origin in disease onset have not
68 yet been studied for NUP98::KDM5A.

69 Fetal and adult hematopoiesis differ in various important aspects [19, 20]. First of all,
70 cellular composition of fetal liver hematopoiesis is vastly different from the adult bone
71 marrow with a skewing for erythro-megakaryocytic output [9, 21]. More importantly,
72 fetal hematopoietic stem cells are highly proliferative and self-renewing when building
73 the stem cell pool for lifelong support of blood formation, whereas the adult
74 counterparts are quiescent to maintain genomic integrity [21-23]. Molecularly, these
75 distinctions are coordinated by diverging epigenetic – and resulting transcriptional –
76 programs.

77 Here, we show that fetal ontogeny contributes to the aggressiveness of
78 NUP98::KDM5A AML in part by sustaining a TRIP13/PPM1D-TP53 survival axis, and
79 we exploit this vulnerability through direct TRIP13 inhibition or a readily translatable
80 idasanutlin–navitoclax–5-azacytidine combination.

81 Results

82 NUP98::KDM5A induces aggressive leukemia in fetal HSPCs

83 To identify the impact of ontogeny in NUP98::KDM5A-driven leukemia, we generated
84 matched fetal and adult murine cell models for NUP98::KDM5A AML. Murine
85 Hematopoietic Stem and Progenitor Cells (HSPCs) were isolated from fetal liver of
86 healthy fetuses at E13.5 (mFL-HSPCs) and from bone marrow of adult mice (mBM-
87 HSPCs) and then transduced with a lentiviral vector expressing the human
88 NUP98::KDM5A cDNA [24] and EGFP (Fig. 1a). Both adult and fetal cells showed a
89 progressive outgrowth of NUP98::KDM5A^{+} GFP^{+} cells indicative of transformation,

90 whereas control vector transduced cells exhausted over time (Fig. 1b and
91 Supplementary Fig. 1a). Despite comparable transduction rates and similar
92 immunophenotype, fetal NUP98::KDM5A$^+$ cells outcompeted the untransduced
93 HSPCs significantly faster than the adult NUP98::KDM5A$^+$ cells (Fig. 1b and
94 Supplementary Fig. 1a).

95 Immunophenotypic analysis revealed that NUP98::KDM5A expression maintained
96 cells in an immature LSK (Lineage$^-$ c-Kit$^+$ Sca1$^+$) state with maturation arrest,
97 corroborated by cytology (Fig. 1c-d and Supplementary Fig. 1b) and transcriptional
98 profiling (Supplementary Fig. 1c and Supplementary Table 3). CIBERSORT [25, 26]
99 deconvolution of bulk RNA-seq revealed that fetal NUP98::KDM5A cells showed a
100 significantly higher proportion of immature progenitors relative to control cells, an
101 effect not observed in the adult counterpart (Fig. 1e). Gene expression analysis
102 confirmed that fetal NUP98::KDM5A$^+$ cells retained fetal signatures compared to adult
103 cells (Fig. 1f and Supplementary Table 4). As expected, both models exhibited
104 upregulation of *HOXA* and *HOXB* gene clusters and marked downregulation of *RB1*
105 target genes (Supplementary Fig. 1c and Supplementary Table 3), consistent with a
106 transcriptional program resembling the RB1-mutant state frequently co-occurring in
107 NUP98::KDM5A AML [12, 15, 27].

108 *In vivo*, transplantation of fetal NUP98::KDM5A$^+$ cells into syngeneic recipients
109 resulted in significantly accelerated leukemia development compared to adult-derived
110 cells (latency fetal: 36 days; adult: 70 days; median disease-free survival; $P_{log\ rank}$
111 =1.068e-005; Fig. 1g). Splenomegaly was significantly more pronounced in mice
112 receiving fetal NUP98::KDM5A$^+$ cells (Fig. 1h). Leukemic blasts in the bone marrow
113 expressed high levels of the mature myeloid surface marker Gr-1 and CD11b (Mac-1),
114 alongside a residual immature LSK fraction (Supplementary Fig. 1d-e).

Our results thus highlight that ontogeny is a key determinant of the aggressivity of NUP98::KDM5A driven AML.

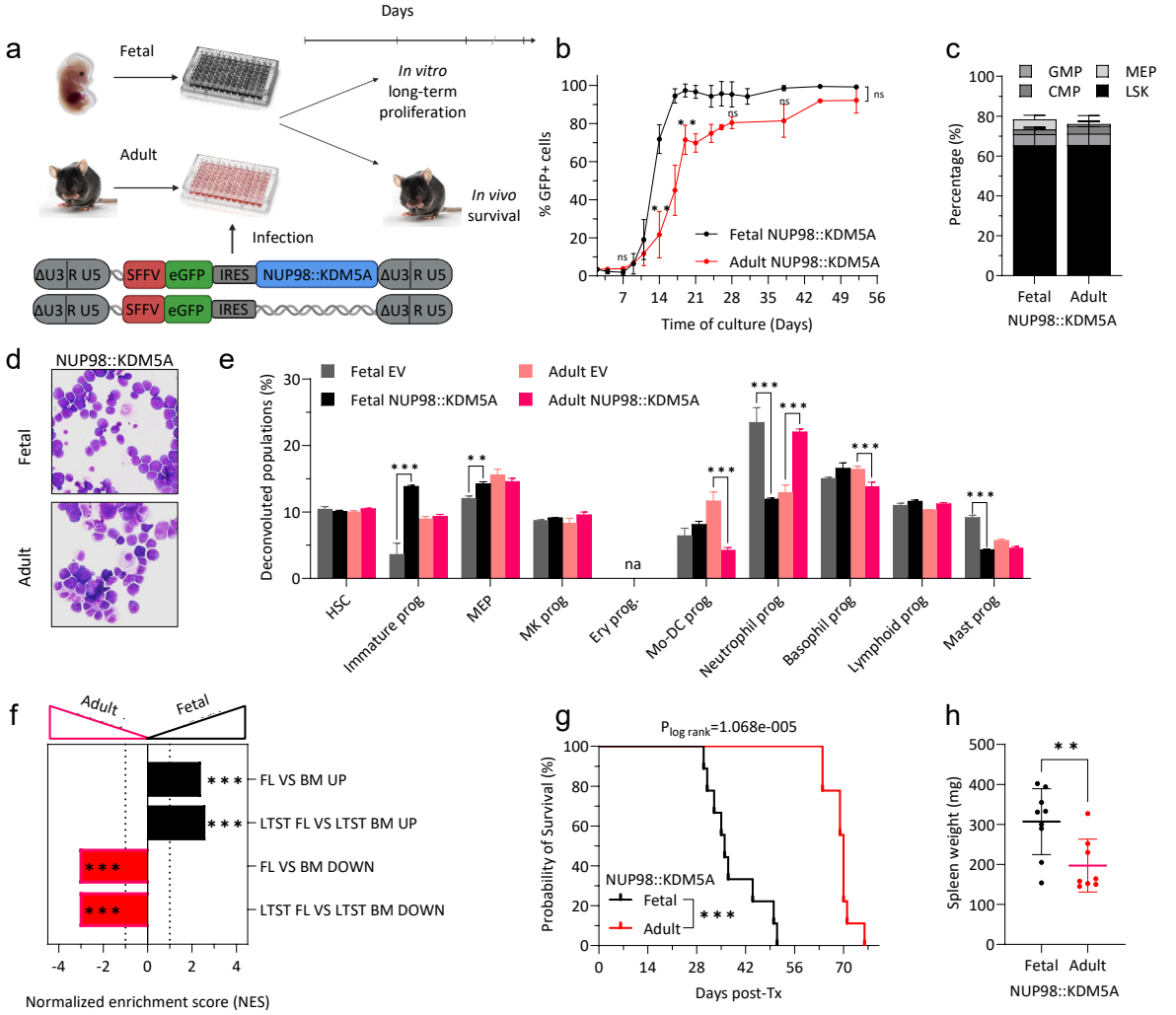

Fig. 1. NUP98::KDM5A fusion oncoprotein induces a more aggressive disease in fetal cells.

a) Schematic workflow for the generation of *in vitro* and *in vivo* murine models of constitutive overexpression of NUP98::KDM5A fusion oncoprotein in murine Hematopoietic Stem and Progenitor Cells (HSPCs) isolated from fetal liver (mFL-HSPCs) of healthy fetuses at E13.5 and bone marrow of adult mice (mBM-HSPCs). Created in Biorender.com
b) GFP+ percentage of fetal and adult NUP98::KDM5A^{+} cells maintained in liquid culture. Data from 1 representative experiment performed in replicates (n > 3) are shown as mean s.d. (t-test).
c) Bar graph showing the percentage of LSK (Lineage negative, c-kit+ and Sca1+), Megakaryocytic-erythroid (MEP; Lineage negative, c-kit+, Sca1-, CD16/CD32- and CD34+) and common myeloid (CMP; Lineage negative, c-kit+, Sca1-, CD16/CD32- and CD34-) and granulocyte/monocyte (CMP; Lineage negative, c-kit+, Sca1-, CD16/CD32+ and CD34+) progenitors of fetal and adult NUP98::KDM5A^{+} cells after 4 weeks of culture. (mean ± s.d., n > 3).
d) Representative cytospin images (x40 original magnification) of fetal and adult NUP98::KDM5A^{+} cells from *in vitro* culture at day 21.

e) Cellular component of bulk RNA samples (n= 3 per condition) inferred by CIBERSORT using signature matrix derived from reference scRNAseq data. Abbreviations. HSC: hematopoietic stem cell, Immature prog: Immature progenitor, MEP: Megakaryocyte–erythroid progenitor, MK prog: Megakaryocyte progenitor, Ery prog: Erythroid progenitor, Mo-DC: Monocyte and Dendritic cell progenitor, Neutrophil prog: Neutrophil progenitor, Basophil prog: Basophil progenitor, Lymphoid prog: Lymphoid progenitor, Mast progenitor: Mastocyte progenitor.
f) Bar graphs showing the normalized enrichment scores (NES) of significantly upregulated or downregulated gene sets in fetal NUP98::KDM5A$^+$ cells compared to adult NUP98::KDM5A$^+$ cells.
g) Kaplan-Meier survival curves of C57BL/6N mice transplanted with fetal and adult NUP98::KDM5A$^+$ cells (n ≥ 6).
h) Dot plot showing spleen weights of C57BL/6N mice transplanted with fetal and adult NUP98::KDM5A$^+$ cells (mean ± s.d., n ≥ 6) (t-test).

ns, not significant * P < .05, ** P < .01, ***P < .001, ****P < .0001

Fetal dependency screening reveals TRIP13 as a critical vulnerability in NUP98::KDM5A$^+$ AML

The aggressive phenotype of fetal-derived NUP98::KDM5A leukemia is closely linked to the persistence of fetal transcriptional programs. These programs create a developmental vulnerability in the post-fetal hematopoietic environment of pediatric patients, where they may be essential for leukemic maintenance and exploitable for therapeutic intervention. To address this, we performed a CRISPR-Cas9 loss of function screen targeting 867 genes, upregulated in human and murine fetal liver HSPCs compared to their adult counterparts [28], in fetal and adult NUP98::KDM5A$^+$ cells (Fig. 2a-b). To achieve selectivity, we complemented the screens with two additional murine AML models – familial-platelet disorder with loss of *Runx1* and *Bcor* (FPD-AML) [29], and myeloid leukemia in Down syndrome (ML-DS) (Fig. 2c and Supplementary Fig. 2a) [30-32]. Applying a depletion cutoff of >70% identified seven candidates, but only the AAA+ (ATPases Associated with diverse cellular Activities) ATPase *Trip13* also exceeded a fetal/adult ratio of >2.5, highlighting it as a particularly compelling and druggable target (Supplementary Fig. 2b). We next validated *Trip13* loss in a single-well fluorescence-based depletion assay with a set of independent gRNAs (Fig. 2d). To corroborate our findings in the context of human leukemia, we

168 knocked out *TRIP13* using the CRISPR-Cas9 system in a broad variety of human
169 leukemic and non-leukemic (HT1080) cell lines, as well as in primary human fetal
170 HSPCs expressing NUP98::KDM5A. Consistent with murine results, *TRIP13* loss
171 markedly impaired the growth of NUP98::KDM5A^{+} human fetal HSPCs, while the
172 proliferation of most control lines was only mildly affected by *TRIP13* loss (Fig. 2e).
173 Gene expression profiling first confirmed that *TRIP13* is upregulated as part of a fetal
174 transcriptional program, being more highly expressed in fetal than in adult HSPCs and
175 in pediatric AMKL compared to adult HSPCs and mature hematopoietic cells (Fig. 2f).
176 Notably, NUP98::KDM5A fusion oncoprotein further reinforced *TRIP13* upregulation in
177 fetal but not in adult cells, revealing a fetal context-specific effect of the fusion on
178 *TRIP13* (Fig. 2g).

179 Altogether, these data point to *TRIP13* as a context-dependent vulnerability that is
180 most evident in fetal-derived and NUP98::KDM5A-positive leukemias, thereby offering
181 a potential target for therapeutic intervention in this high-risk AML subtype.

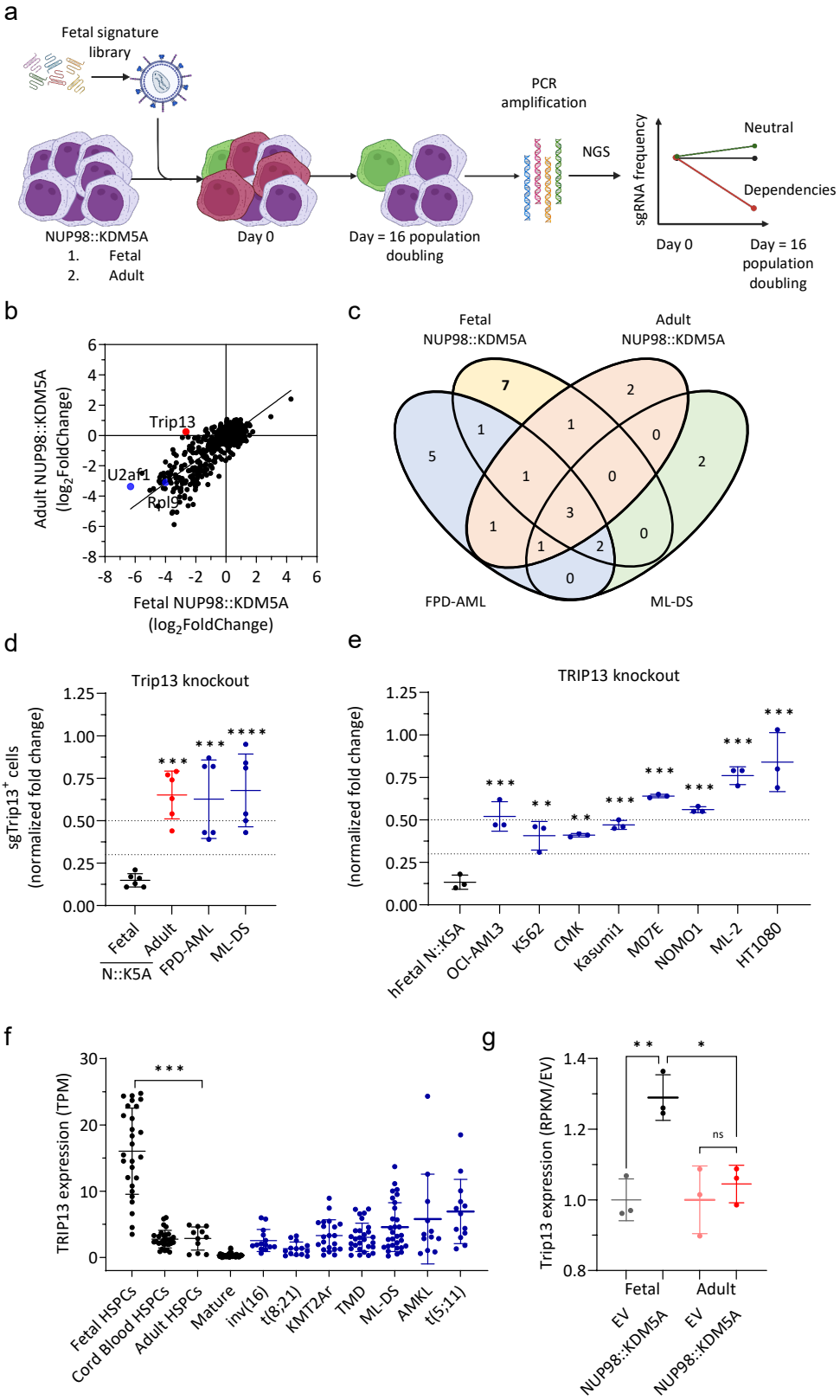

Fig. 2. CRISPR-Cas9 knock-out screening reveals *TRIP13* dependency in fetal NUP98::KDM5A⁺ model.

a) Schematic workflow of the high-throughput fetal signatures-based CRISPR-Cas9 *in vitro* screen.

b) Dot plots showing the log2 fold change of the fetal enriched genes targeted by sgRNAs in fetal (x-axis) and adult (y-axis) NUP98::KDM5A$^+$ models. Blue dots represent positive control (*Rpl9*, *U2af1*). Red dots represent selected candidate gene *Trip13*. (n =2)
c) Venn diagram illustrating significantly (P-value < 0.05) depleted (depletion > 70%) sgRNAs in different murine leukemia models.
d) Dot plot showing the percentage of *Trip13*-targeting sgRNA-transduced fetal, adult NUP98::KDM5A$^+$ (N::K5A), FPD-AML and ML-DS models after 21 days of culture, normalized to (negative control sgRNA [sgCtr]) and to day 2 (mean ± s.d., n > 3 per sgRNA, 1-way ANOVA).
e) Dot plot showing the percentage of *TRIP13*-targeting sgRNA-transduced hFL NUP98::KDM5A$^+$ (N::K5A) cells and leukemia cell lines (OCI-AML3; K562; CMK; Kasumi1; M07E; NOMO1; ML-2) and non-leukemia cell line (HT1080) after 21 days of culture, normalized to (negative control sgRNA [sgCtr] and positive control sgRNA [sgRPL9 and sgU2AF1]) and to day 2 (mean ± s.d., n = 3 per sgRNA, 1-way ANOVA).
f) Dot plot showing the expression of *TRIP13* in subgroups of HSPCs and pediatric AML from the HemAtlas dataset.
g) Dot plot showing the expression of *Trip13* in control (EV) or NUP98::KDM5A$^+$ murine fetal and adult cells after 21 days of culture (n = 3).

ns, not significant * P < .05, ** P < .01, ***P < .001, ****P < .0001.

Trip13 loss triggers TP53-dependent apoptosis

To verify that *Trip13* loss was causative for the observed phenotype, we co-transduced fetal NUP98::KDM5A$^+$ cells with *TRIP13* cDNA and *Trip13*-targeting sgRNAs. *TRIP13* overexpression fully rescued cell depletion, confirming on-target specificity (Fig. 3a). *Trip13* knock-out, validated by Western blotting (Supplementary Fig. 3a), induced pronounced apoptosis (Fig. 3b) and a G_2/M arrest (Fig. 3c), consistent with TRIP13's role in mitotic checkpoint control [33], without altering differentiation status (Supplementary Fig. 3b).

214

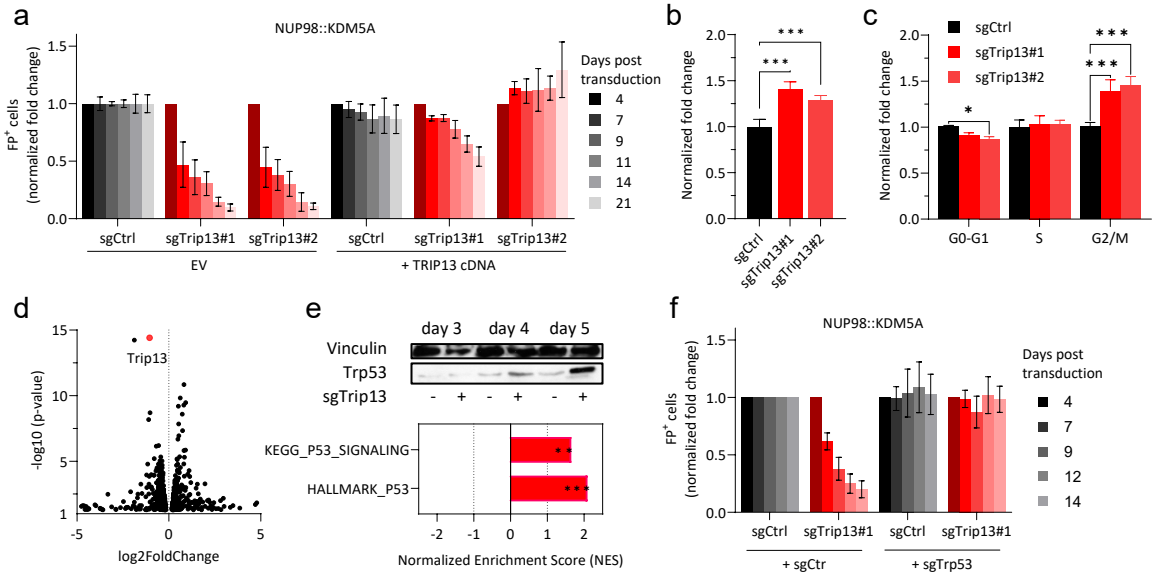

215

216 **Fig. 3. *Trip13* loss promotes activation of the TP53 pathway and arrests fetal**
217 **NUP98::KDM5A⁺ cell proliferation *in vitro*.**

218 a) Bar plot showing the percentage of sgRNA-transduced (negative control sgRNA
219 [sgCtr], sgTrip13#1-2) empty vector (EV) and TRIP13 overexpressing fetal
220 NUP98::KDM5A⁺ cells after 14 days of culture, normalized to day 4 (mean±s.d., n > 3
221 per sgRNA, 1-way ANOVA)
222 b) Bar graphs showing the percentage of Annexin-V⁺ sgRNA-transduced (negative control
223 sgRNA [sgCtr], sgTrip13#1-2) fetal NUP98::KDM5A⁺ cells after 5 days of culture,
224 normalized to control sgRNA (sgCtr) (mean ± s.d., n > 3 per sgRNA, 1-way ANOVA).
225 c) Bar plot showing the percentage of sgRNA-transduced (negative control sgRNA
226 [sgCtr], sgTrip13#1-2) fetal NUP98::KDM5A⁺ cells in G0-G1, S and G2/M phase after
227 5 days of culture (mean ± s.d., n > 3 per sgRNA, 2-way ANOVA).
228 d) Volcano plot showing the differentially expressed genes upon *Trip13* knock-out in fetal
229 NUP98::KDM5A⁺ cells P-value < 0.05 (n = 3). RNA-seq-based gene expression
230 analysis of sgRNA-transduced (negative control sgRNA [sgCtr], sgTrip13#1) fetal
231 NUP98::KDM5A⁺ cells was performed after 4 days of culture.
232 e) Timeline Western blot showing TP53 protein levels in sorted sgRNA-transduced
233 (negative control sgRNA [Luc], sgTrip13#1) fetal NUP98::KDM5A⁺ cells 4 days after
234 transduction. Endogenous Vinculin was used as loading control.
235 Bar graphs showing the normalized enrichment scores (NES) of significantly
236 deregulated gene sets associated with TP53 pathway in *Trip13* knock-out fetal
237 NUP98::KDM5A⁺ cells compared to control sgRNA.
238 f) Bar plot showing the percentage of sgRNA-transduced (negative control sgRNA
239 [sgCtr], sgTrip13, sgTrp53) fetal NUP98::KDM5A⁺ cells after 14 days of culture,
240 normalized to day 4 (mean±s.d., n > 3 per sgRNA, 1-way ANOVA)

241 ns, not significant * P < .05, ** P < .01, ***P < .001, ****P < .0001.

242 Aiming for the molecular mechanisms underlying *Trip13* dependency, we measured
243 gene expression changes 4 days after CRISPR-Cas9 induced TRIP13 knock-out in
244 fetal NUP98::KDM5A⁺ cells (Fig. 3d). Surprisingly, gene set enrichment analysis

245 (GSEA [34]) revealed that upon *Trip13* knock-out was exclusively associated with
246 perturbations of the TP53 signaling pathway (Fig. 3e and Supplementary Fig. 3c,
247 Supplementary Table 5). In line with this, TP53 protein levels were increased in a time-
248 dependent manner upon *Trip13* knock-out (Fig. 3e), and co-deletion of *Trp53*
249 completely rescued the growth defect induced by *Trip13* loss (Fig. 3f), demonstrating
250 that TP53 activation mediates the *Trip13* dependency in fetal NUP98::KDM5A$^+$ AML
251 cells. Several studies have shown that TRIP13 is involved in the regulation of DNA
252 damage repair [35, 36]. To determine whether DNA damage contributes to TP53
253 activation and cell death, we measured γH2AX protein levels by Western blotting.
254 Although basal DNA damage was detected, *Trip13* deletion did not further increase
255 γH2AX levels in fetal NUP98::KDM5A$^+$ cells versus controls (Supplementary Fig. 3d),
256 suggesting that TP53 induction following *Trip13* loss occurred independently of
257 additional genotoxic stress.

258 Together, these results establish that fetal *NUP98::KDM5A*$^+$ AML cells are sensitive to
259 TP53 activation and that *Trip13* maintains leukemic survival by suppressing TP53,
260 independently of DNA damage signaling.

261 **TRIP13 interacts with PPM1D/WIP1 to repress TP53 pathway activation**

262 To further understand how TRIP13 regulates TP53, we mapped its protein-protein
263 interaction network via co-immunoprecipitation followed by mass spectrometry (IP-MS)
264 using doxycycline-inducible hemagglutinin (HA)-tagged TRIP3 in a TP53 wild-type
265 leukemia cell line (OCI-AML3) (Fig. 4a) [37, 38]. Among the proteins identified by
266 TRIP13 pull-down, we focused on 33 candidates previously annotated in STRING as
267 having functional or physical connection to TP53 (Fig. 4b). To investigate which of
268 these candidate genes mediate the *Trip13*-dependency we used a functional
269 approach. We hypothesized that the knock-out of a Trip13-interactor that is relevant

for TP53 suppression would mimic the effect of *Trip13* knock-out, thus leading to a proliferative disadvantage in NUP98::KDM5A^{+} cells that is rescued by *Trp53* co-deletion. Out of the 33 candidates, the knock-out of 16 Trip13-interactors caused a similar depletion rate as *Trip13* loss (Supplementary Fig. 4a). As *Trp53* knock-out rescues the effect of Trip13 loss, we next systematically combined *Trp53* knock-out with each of these 16 Trip13-interactors (Supplementary Fig. 4b). Upon Trp53 co-deletion, the protein phosphatase PPM1D/WIP1, a well-known regulator of TP53 in a direct and indirect manner via MDM2 stabilization, stood out as the top TRIP13 interactor (Fig. 4c and Supplementary Fig. 4b) [39]. Both *Trip13* and *Ppm1d* knock-out in fetal NUP98::KDM5A^{+} cells induced elevated TP53 protein levels (Fig. 4d). Co-immunoprecipitation of TRIP13 and Western blotting confirmed the TRIP13-PPM1D interaction in OCI-AML3 cells (Fig. 4e). Of note, *PPM1D/WIP1* expression – like TRIP13 – was elevated in pediatric AMKL patients compared to adult HSPCs and mature hematopoietic cells (Supplementary Fig. 4c).

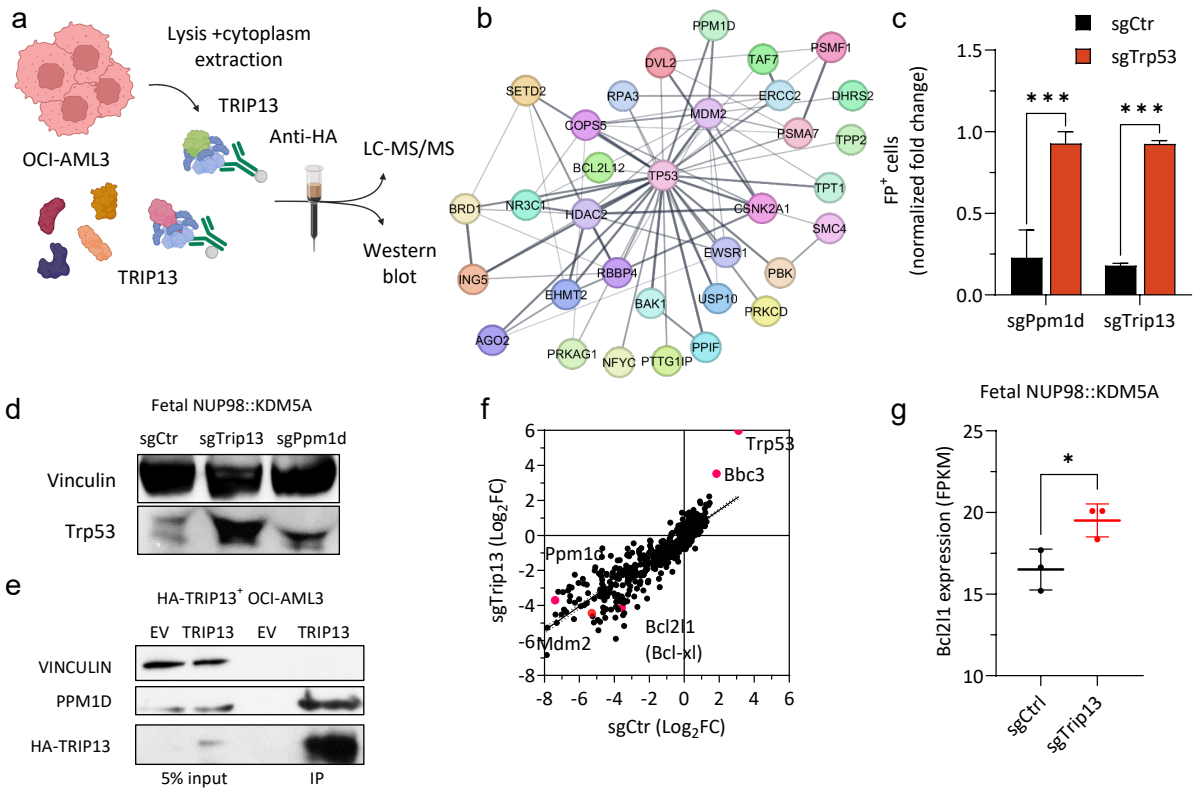

Fig. 4 TRIP13 interacts with PPM1D/WIP1 to repress the TP53 pathway.

a) Experimental workflow for isolating HA-tagged TRIP13 protein and its interactors from OCI-AML3 cells.
b) String protein-protein interaction network of 33 TRIP13-interacting candidates. Network nodes (colored circles) represent proteins, lines between the nodes (edges) indicate the different types of interaction (functional and physical protein associations), the line thickness indicates the confidence of interaction (0.4).
c) Bar plot showing the percentage of sgRNA-transduced (sgPpm1d, sgTrip13) fetal NUP98::KDM5A$^+$ cells in combination with negative control sgrna [sgCtr] or sgTrp53 after 14 days of culture, normalized to day 2 (mean±s.d., n > 3 per sgRNA, 1-way ANOVA)
d) Western blot showing TP53 protein levels in sorted sgRNA-transduced (negative control sgRNA [Luc], sgTrip13 and sgPpm1d) fetal NUP98::KDM5A$^+$ cells 4 days after transduction. Endogenous Vinculin was used as loading control.
e) Western blot showing co-immunoprecipitation of PPP1D after HA-pulldown of HA-tagged TRIP13 in OCI-AML3 cells. Endogenous Vinculin was used as loading control.
f) Dot plots showing the log2 fold change of the TP53 pathway-related genes targeted by control (x-axis), *Trip13*-depleted (y-axis) fetal NUP98::KDM5A$^+$ cells. Red dots represent selected candidate genes (*Ppm1d*, *Mdm2*, *Bcl2l1*, *Bbc3*, *Trp53*). (n = 2)
g) Dot plot showing the expression of *Bcl2l1* of control or *Trip13*-depleted fetal NUP98::KDM5A$^+$ cells after 4 days of culture (n = 3).

ns, not significant * P < .05, ** P < .01, ***P < .001, ****P < .0001.

To gain more insights into the function of *Trip13* in the TP53 signaling network, we performed a CRISPR-Cas9 knock-out screen of 704 TP53-pathway genes in fetal NUP98::KDM5A$^+$ cells, with or without *Trip13* knockout (Fig. 4f). Ablation of *Trp53* or *Bbc3/Puma* led to a strong enrichment of their corresponding sgRNAs in the CRISPR screen, indicating that mitochondrial apoptosis represents the predominant cell death mechanism induced upon *Trip13* loss. Additionally, knock-out of *Mdm2* and *Bcl-xl/Bcl2l1* enhanced the antiproliferative effects of *Trip13* ablation, suggesting a potential therapeutic synergy (Fig. 4f). Notably, *Bcl-xl* and *Bbc3* expression was further elevated upon *Trip13* loss, indicating a feedback loop through which the cells attempt to evade apoptosis (Fig. 4g and Supplementary Fig. 4d).

Thus, our proteomic and functional data show that TRIP13 binds to PPM1D, and both contribute to the suppression of TP53 activation in fetal NUP98::KDM5A$^+$ cells, which can be reversed by inhibiting MDM2 and BCL-XL.

Therapeutic Targeting of TRIP13 Reactivates TP53 in NUP98::KDM5A$^+$ AML

320 Our combined proteomic and genomic analyses identified TRIP13 as a critical
321 suppressor of TP53 in fetal NUP98::KDM5A$^+$ AML, suggesting that pharmacological
322 TRIP13 inhibition could be a therapeutic option [40].

323 Treatment with the experimental small molecule TRIP13 inhibitor DCZ0415 replicated
324 *Trip13* loss and robustly induced apoptosis in NUP98:KDM5A$^+$ cells in a dose-
325 dependent manner (mean IC_{50} fetal = 22 μM, adult = 26 μM). NUP98::KDM5A cells
326 were significantly more sensitive than FPD-AML, ML-DS or mBM-HSPC cells (mean
327 $IC_{50:}$ FPD-AML: 50 μM, ML-DS: 35 μM, mBM-HSPCs: 45 μM) (Fig. 5a and
328 Supplementary Fig. 5a-b). Human fetal NUP98::KDM5A$^+$ cells were similarly sensitive
329 to DCZ0415 (mean IC_{50} = 19 μM), while OCI-AML3, Kasumi1 or M07E showed lower
330 or only partial response (IC_{50}: OCI-AML3: 32 μM, Kasumi-1/M07e: NM = not
331 measurable; Fig. 5b and Supplementary Fig. 5c). DCZ0415 treatment caused
332 activation of the TP53 pathway and induced cell death, which could be rescued both
333 by overexpressing TRIP13 or by knocking out *Trp53* (Fig. 5c, Supplementary Fig. 5d
334 and Supplementary Table 5).

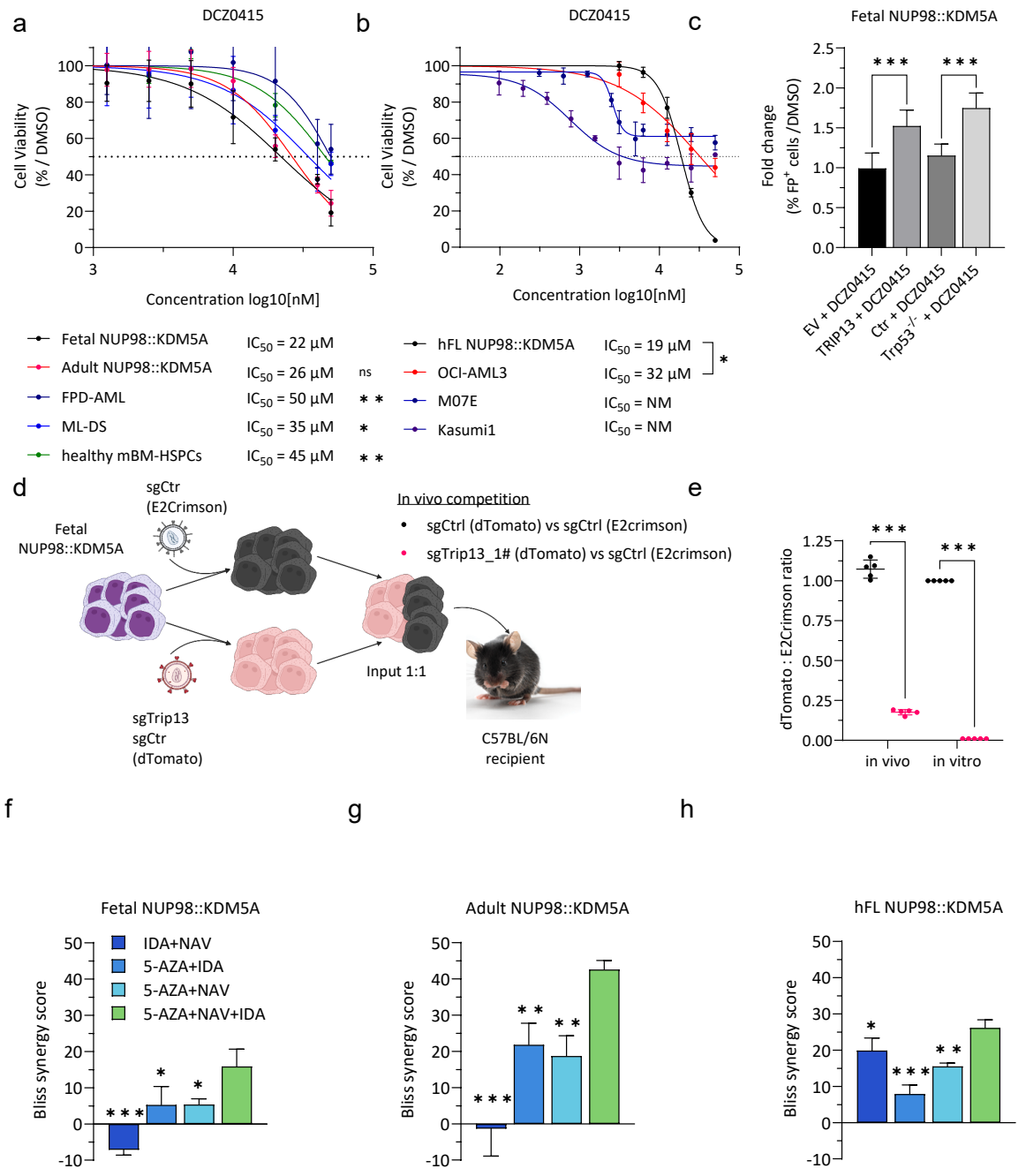

Fig. 5. Pharmacological inhibition of TRIP13-TP53 axis is a therapeutic option for NUP98::KDM5A⁺ pediatric leukemia.

a) Dose-response curves for DCZ0415 (TRIP13 inhibitor) in fetal and adult NUP98::KDM5A⁺, ML-DS and FPD-AML models and healthy mBM-HSPCs after 5 days of treatment *in vitro*. The corresponding IC_{50}-values are depicted below the graphs. (mean ± s.d. , n > 3, 1-way ANOVA related to fetal NUP98::KDM5A⁺ cells)

b) Dose-response curves for DCZ0415 (TRIP13 inhibitor) in hFL NUP98::KDM5A⁺ cells and OCI-AML3, M07E and Kasumi1 after 5 days of treatment *in vitro*. The corresponding IC_{50}-values are depicted below the graphs. (mean ± s.d. , n > 3, 1-way ANOVA related to hFL NUP98::KDM5A⁺ cells).

c) Bar graphs showing the percentage of sgRNA-transduced (negative control sgRNA [sgCtr], sgTrp53) and empty vector (EV) or TRIP13-overexpressing fetal NUP98::KDM5A⁺ cells after 7 days of treatment with DCZ0415 (TRIP13 inhibitor) *in vitro*. (mean±s.d. , n > 3, 1-way ANOVA).

d) Experimental setup for evaluating the genetic ablation of *Trip13* in fetal NUP98::KDM5A$^+$ cells *in vivo*. Fetal NUP98::KDM5A$^+$ cells (with stable Cas9 expression) were co-transduced with sgTrip13 (dTomato) and sgCtr (dTomato) and mixed 1:1 with sgCtr (E2Crimson), before transplantation into sublethally irradiated recipient mice.
e) Dot plot showing the ratio of dTomato$^+$ to E2Crimson$^+$ cells in the bone marrow of mice euthanized 4 weeks after transplantation (n = 5) and after 4 weeks of culture, normalized to day 0 (n = 3, 2-way ANOVA)
f) Bar plot showing the summary Bliss synergy score of double or triple combinatorial treatment with drugs (IDA = idasanutlin, NAV = navitoclax, 5-AZA = 5-azacytidine) of fetal NUP98::KDM5A$^+$ cells after 5 days. (mean ± s.d. , n = 3, 1-way ANOVA related to the triple combination)
g) Bar plot showing the summary Bliss synergy score of double or triple combinatorial treatment with drugs (IDA = idasanutlin, NAV = navitoclax, 5-AZA = 5-azacytidine) of adult NUP98::KDM5A$^+$ cells after 5 days. (mean ± s.d. , n = 3, 1-way ANOVA related to the triple combination)
h) Bar plot showing the summary Bliss synergy score of double or triple combinatorial treatment with drugs (IDA = idasanutlin, NAV = navitoclax, 5-AZA = 5-azacytidine) of hFL NUP98::KDM5A$^+$ cells after 5 days. (mean ± s.d. , n >=3, 1-way ANOVA related to the triple combination)

ns, not significant * P < .05, ** P < .01, ***P < .001, ****P < .0001.

Lastly, we evaluated *Trip13* knock-out *in vivo* through fluorescence-based competitive transplantation assays using fetal NUP98::KDM5A$^+$ cells (Fig. 5d). *Trip13*-depleted leukemic blasts were significantly diminished in the bone marrow of recipient mice at the experimental endpoint, consistent with *in vitro* findings (Fig. 5e).

These results establish that TRIP13 inhibition predominantly affects NUP98::KDM5A$^+$ leukemic cell survival by reactivating TP53 signaling, supporting its development as a targeted therapeutic strategy for this high-risk pediatric AML subtype.

A clinically applicable intervention exploiting TP53 sensitivity in NUP98::KDM5A-driven AML

As TRIP13 inhibitors are still in early development, thus prohibiting clinical translation at this stage [41, 42], we sought to pharmacologically mimic TRIP13 loss using TP53-reactivating drugs that are approved or in late-stage clinical trials. Our TP53 pathway CRISPR screening suggested *MDM2* and *BCL2L1* as promising candidates (Fig. 4f). The MDM2 inhibitor idasanutlin [43] induced dose-dependent apoptosis in both fetal and adult NUP98::KDM5A$^+$ cells, whereas the BCL2/BCL-XL inhibitor navitoclax [44,

385 45] was active only in fetal cells, with partial effects in adult NUP98::KDM5A$^+$, FPD-
386 AML, and ML-DS models (Supplementary Fig. 5e-h).

387 Consequently, we performed combined treatment with idasanutlin and navitoclax but
388 could not detect any synergistic activity (Fig. 5f-h). Notably, combined treatment with
389 DCZ0415 and idasanutlin or navitoclax resulted in synergistic killing of fetal
390 NUP98::KDM5A$^+$ cells (Supplementary Fig. 5i), indicating that additional triggers are
391 needed to mimic the effect of TRIP13 inhibition. Given the established role of
392 hypomethylating agents as a chemotherapy sensitizer [46-48], we incorporated 5-
393 azacytidine (5-AZA) into the idasanutlin-navitoclax regimen. This triple combination
394 produced robust synergy in fetal, adult, and human fetal NUP98::KDM5A$^+$ cells (Bliss
395 synergy scores: 16, 43, and 26, respectively) and was broadly active across models
396 (Fig. 5f-h).

397 Hence, our clinically applicable strategy for TP53 reactivation, using a combination of
398 the FDA-approved drugs idasanutlin and 5-azacytidine along with the investigational
399 agent navitoclax, offers promising therapeutic options for rapid translation into early-
400 phase trials in NUP98::KDM5A$^+$ AML.

401 Discussion

402 In this study, we identified a novel therapeutic vulnerability in infant leukemia by
403 interrogating the developmental basis of the disease, moving beyond an oncogene-
404 centric framework. This ontogeny-focused approach revealed a targetable
405 dependency linked to fetal hematopoiesis and may represent a paradigm shift for other
406 malignancies with marked developmental origin. NUP98::KDM5A-rearranged AML is
407 a rare but highly aggressive subtype that occurs predominantly in infants and very
408 young children below the age of 2 years [6-8]. Its early occurrence strongly suggests

409 that leukemia initiates during embryogenesis [49], implicating the unique biology of
410 fetal hematopoiesis in disease development. Even with intensive chemotherapy and
411 allogeneic hematopoietic stem cell transplantation (HSCT), outcomes remain poor,
412 relapses are frequent and high treatment-related morbidity is observed. Achieving
413 deep, MRD-negative remissions prior to HSCT is a critical determinant of long-term
414 survival, yet current induction regimens are often too toxic or ineffective for this fragile
415 patient population [50].
416 While ontogeny has increasingly gained recognition in other pediatric hematologic
417 malignancies, including CBFA2T3::GLIS2 and KMT2A-rearranged leukemias [6], its
418 impact in NUP98::KDM5A-driven AML has not been directly addressed. Using
419 matched fetal and adult HSPC models, we demonstrate that NUP98::KDM5A-driven
420 AML arising in a fetal context is more aggressive and retains ontogeny-specific
421 transcriptional programs [19, 20, 51]. Functional genomic interrogation of fetal-
422 enriched genes identified TRIP13 – a AAA^+ ATPase and direct interactor of the TP53
423 phosphatase PPM1D/WIP1 – as a critical dependency in fetal NUP98::$KDM5A^+$ cells.
424 TRIP13 suppresses TP53 activation, and its loss or inhibition reactivates TP53
425 signaling, triggering G_2/M arrest and mitochondrial apoptosis without additional DNA
426 damage [33, 35]. Our findings suggest that TRIP13 mitigates NUP98::KDM5A-induced
427 DNA stress [52] by modulating TP53 activity, potentially by its physical interaction with
428 PPM1D, a well-established oncogenic suppressor of TP53 [53]. The precise
429 mechanism by which TRIP13 may regulate PPM1D activity remains to be defined.
430 Given that TRIP13 has been reported to remodel protein conformation through its
431 ATPase function [54], it is plausible that TRIP13 similarly modulates PPM1D
432 conformation to influence its phosphatase activity. Mechanistically, this positions TP53
433 repression via TRIP13/PPM1D at the core of leukemic maintenance and links it to the

434 oncofetal transcriptional programs induced -at least partially- by NUP98::KDM5A [52,
435 55].
436 While we cannot yet determine whether these programs reflect direct binding of
437 NUP98::KDM5A to oncofetal genes or secondary downstream effects, a recent study
438 indentified developmental and oncofetal genes such as *Nkx2-3* and *Igf2bp3* as direct
439 targets of NUP98::KDM5A, supporting our hypothesis of a direct role of
440 NUP98::KDM5A in fetal gene activation [52]**.**
441 Prior mechanistic studies of NUP98::KDM5A-driven leukemia have uncovered
442 dependencies such as the MEN–KMT2A axis, CDK6, and CDK12 [51, 52, 55] , all of
443 which converge on sustaining active transcription and cell-cycle progression.
444 Such enforced proliferation and DNA replication intrinsically promote DNA damage
445 [56], consistent with reports that NUP98::KDM5A-expressing cells exhibit high levels
446 of DNA repair machinery, baseline DNA damage, and heightened sensitivity to
447 CDK12/13 inhibition [52, 57]. Coping with this DNA stress and avoiding apoptosis
448 appear to be central requirement of transformation, which we show involves TRIP13
449 acting through PPM1D to maintain low levels of TP53. Notably, the DNA damage–
450 related genes identified in our CRISPR–Cas9 screens were also reported by Troester
451 et al. [52] as maintained by *NUP98::KDM5A* and are upregulated during fetal
452 development, further aligning our findings with theirs. While PPM1D is the prime TP53-
453 modulating factor interacting with TRIP13 in our system, our protein-protein interaction
454 analysis revealed numerous additional TP53 network components interacting with
455 TRIP13, including 16 candidates whose perturbation partially phenocopied the TP53-
456 dependent depletion seen upon Trip13 loss. This multimodal regulation likely explains
457 the higher TP53 levels in *Trip13* knock-out compared to *Ppm1d* knock-out cells,
458 underscoring the complexity of TRIP13-mediated TP53 control.

459 Importantly, our work provides proof- of- concept for pharmacologic inhibition of
460 TRIP13 using the small-molecule inhibitor DCZ0415, which faithfully recapitulated the
461 effects of genetic TRIP13 loss, inducing TP53-dependent apoptosis in
462 NUP98::KDM5A^{+} AML cells. Although DCZ0415 is not yet clinically deployable, these
463 findings underscore the potential of TRIP13 as a druggable target in high-risk pediatric
464 AML and warrant the development of next-generation inhibitors suitable for clinical
465 testing.
466 To bridge the gap until such agents become available, our TP53-pathway CRISPR
467 screen identified MDM2 and BCL2L1 (BCL-XL) as actionable co-targets [58].
468 Unpublished work from our lab and a previous study also demonstrated a molecular
469 dependency on BCL-XL and resistance to BCL2-inhibition (data not shown) in AMKL,
470 in particular in the presence of CBFA2T3::GLIS2 translocation [59]. Our results validate
471 and extend these findings to other fusions, including NUP98-translocated pediatric
472 leukemia, while the loss of BBC3 and TP53 expectedly counteracts this mechanism
473 [60, 61]. Guided by these insights, we designed a triple combination of idasanutlin
474 (MDM2 inhibitor), navitoclax (BCL2/BCL-XL inhibitor), and 5-azacytidine
475 (hypomethylating sensitizer [62]). This regimen phenocopied *TRIP13* loss and
476 triggered robust, synergistic apoptosis across fetal, adult, and human fetal
477 NUP98::KDM5A^{+} AML cells. Importantly, all three agents are FDA-approved or in
478 advanced clinical testing, enabling rapid translational potential.
479 Comparative studies in established murine AML models [30] revealed that, while this
480 pharmacologic strategy exhibited broader activity and less specificity than TRIP13
481 depletion, it nonetheless produced potent antileukemic effects. This difference likely
482 reflects non-identical mechanisms of TP53 engagement by idasanutlin versus TRIP13
483 inhibition, consistent with the observed synergy between both approaches. From a
484 therapeutic standpoint, such broader activity may represent an advantage, potentially

extending benefit beyond NUP98-rearranged disease to other pediatric and adult AML subtypes, though further validation is needed.

Clinically, this mechanism-based regimen could serve as an induction or re-induction strategy to achieve deep remission without the toxicity of additional intensive chemotherapy. Reactivating TP53 and priming apoptosis could promote an optimal remission status before HSCT, offering a tangible opportunity to improve cure rates in NUP98::KDM5A-driven AML. By enhancing both disease clearance and pre-transplant fitness, this strategy could improve HSCT outcomes in a population with otherwise dismal survival rates.

Current treatment paradigms for high-risk, relapsed or refractory pediatric AML – particularly in infants – rely on intensified cytarabine- or fludarabine-based chemotherapy, often combined with anthracyclines or narrow-spectrum targeted agents [63]. While these regimens can achieve remission, they also entail substantial toxicity, prolonged myelosuppression, and high treatment-related morbidity, frequently delaying or precluding HSCT. In contrast, therapeutic strategies targeting the TRIP13-TP53-axis directly with novel TRIP13 inhibitors, or indirectly through the idasanutlin–navitoclax–5-azacytidine combination, offer a targeted, potentially less intensive yet mechanistically potent alternative, distinct from other novel approaches such as those targeting the Menin–KMT2A axis [51, 52, 55]. Reactivating TP53 and priming apoptosis could promote an optimal remission status before HSCT, offering a tangible opportunity to improve cure rates in NUP98::KDM5A-driven AML.

More broadly, our work illustrates how systematic functional interrogation of ontogeny-specific programs can uncover lineage- and age-dependent vulnerabilities invisible to purely mutation-focused analyses. In NUP98::KDM5A^{+} AML, this strategy exposed a central TRIP13/PPM1D–TP53 survival axis, validated TRIP13 as a direct therapeutic target, and delivered an immediately translatable combination regimen that mimics its

511 inhibition. This paradigm – leveraging developmental biology to expose unique,
512 druggable dependencies – may prove transformative for other aggressive pediatric
513 cancers with developmental origins.

514 # References

515 1. Bolouri, H., et al., *The molecular landscape of pediatric acute myeloid leukemia reveals*
516 *recurrent structural alterations and age-specific mutational interactions.* Nat Med, 2018. **24**(1):
517 p. 103-112.
518 2. Papaemmanuil, E., et al., *Genomic Classification and Prognosis in Acute Myeloid Leukemia.* N
519 Engl J Med, 2016. **374**(23): p. 2209-2221.
520 3. Marceau-Renaut, A., et al., *Molecular Profiling Defines Distinct Prognostic Subgroups in*
521 *Childhood AML: A Report From the French ELAM02 Study Group.* Hemasphere, 2018. **2**(1): p.
522 e31.
523 4. Reinhardt, D., E. Antoniou, and K. Waack, *Pediatric Acute Myeloid Leukemia-Past, Present, and*
524 *Future.* J Clin Med, 2022. **11**(3).
525 5. Elgarten, C.W. and R. Aplenc, *Pediatric acute myeloid leukemia: updates on biology, risk*
526 *stratification, and therapy.* Current Opinion in Pediatrics, 2020. **32**(1): p. 57-66.
527 6. Lopez, C.K., et al., *Ontogenic Changes in Hematopoietic Hierarchy Determine Pediatric*
528 *Specificity and Disease Phenotype in Fusion Oncogene-Driven Myeloid Leukemia.* Cancer
529 Discov, 2019. **9**(12): p. 1736-1753.
530 7. Okeyo-Owuor, T., et al., *The efficiency of murine MLL-ENL-driven leukemia initiation changes*
531 *with age and peaks during neonatal development.* Blood Adv, 2019. **3**(15): p. 2388-2399.
532 8. Calvi, L.M. and D.C. Link, *The hematopoietic stem cell niche in homeostasis and disease.* Blood,
533 2015. **126**(22): p. 2443-51.
534 9. Mack, R., et al., *The Fetal-to-Adult Hematopoietic Stem Cell Transition and its Role in Childhood*
535 *Hematopoietic Malignancies.* Stem Cell Rev Rep, 2021. **17**(6): p. 2059-2080.
536 10. de Smith, A.J. and L.G. Spector, *In Utero Origins of Acute Leukemia in Children.* Biomedicines,
537 2024. **12**(1).
538 11. Gruber, T.A. and J.R. Downing, *The biology of pediatric acute megakaryoblastic leukemia.*
539 Blood, 2015. **126**(8): p. 943-9.
540 12. de Rooij, J.D., et al., *Pediatric non-Down syndrome acute megakaryoblastic leukemia is*
541 *characterized by distinct genomic subsets with varying outcomes.* Nat Genet, 2017. **49**(3): p.
542 451-456.
543 13. de Rooij, J.D., et al., *Recurrent abnormalities can be used for risk group stratification in*
544 *pediatric AMKL: a retrospective intergroup study.* Blood, 2016. **127**(26): p. 3424-30.
545 14. Gough, S.M., C.I. Slape, and P.D. Aplan, *NUP98 gene fusions and hematopoietic malignancies:*
546 *common themes and new biologic insights.* Blood, 2011. **118**(24): p. 6247-57.
547 15. Bertrums, E.J.M., et al., *Comprehensive molecular and clinical characterization of NUP98*
548 *fusions in pediatric acute myeloid leukemia.* Haematologica, 2023.
549 16. Gough, S.M., et al., *NUP98-PHF23 is a chromatin-modifying oncoprotein that causes a wide*
550 *array of leukemias sensitive to inhibition of PHD histone reader function.* Cancer Discov, 2014.
551 **4**(5): p. 564-77.
552 17. Wang, G.G., et al., *Haematopoietic malignancies caused by dysregulation of a chromatin-*
553 *binding PHD finger.* Nature, 2009. **459**(7248): p. 847-51.
554 18. Wang, G.G., et al., *NUP98-NSD1 links H3K36 methylation to Hox-A gene activation and*
555 *leukaemogenesis.* Nat Cell Biol, 2007. **9**(7): p. 804-12.
556 19. Roy, A., et al., *Transitions in lineage specification and gene regulatory networks in*
557 *hematopoietic stem/progenitor cells over human development.* Cell Rep, 2021. **36**(11): p.
558 109698.
559 20. Ivanovs, A., et al., *Human haematopoietic stem cell development: from the embryo to the dish.*
560 Development, 2017. **144**(13): p. 2323-2337.
561 21. Popescu, D.M., et al., *Decoding human fetal liver haematopoiesis.* Nature, 2019. **574**(7778): p.
562 365-371.
563 22. Bowie, M.B., et al., *Identification of a new intrinsically timed developmental checkpoint that*
564 *reprograms key hematopoietic stem cell properties.* Proc Natl Acad Sci U S A, 2007. **104**(14): p.
565 5878-82.

566 23. Ranzoni, A.M., et al., *Integrative Single-Cell RNA-Seq and ATAC-Seq Analysis of Human*
567 *Developmental Hematopoiesis.* Cell Stem Cell, 2021. **28**(3): p. 472-487.e7.
568 24. de Rooij, J.D., et al., *NUP98/JARID1A is a novel recurrent abnormality in pediatric acute*
569 *megakaryoblastic leukemia with a distinct HOX gene expression pattern.* Leukemia, 2013.
570 **27**(12): p. 2280-8.
571 25. Newman, A.M., et al., *Determining cell type abundance and expression from bulk tissues with*
572 *digital cytometry.* Nat Biotechnol, 2019. **37**(7): p. 773-782.
573 26. Dahlin, J.S., et al., *A single-cell hematopoietic landscape resolves 8 lineage trajectories and*
574 *defects in Kit mutant mice.* Blood, 2018. **131**(21): p. e1-e11.
575 27. Noort, S., et al., *The clinical and biological characteristics of NUP98-KDM5A in pediatric acute*
576 *myeloid leukemia.* Haematologica, 2021. **106**(2): p. 630-634.
577 28. Schwarzer, A., et al., *The non-coding RNA landscape of human hematopoiesis and leukemia.*
578 Nat Commun, 2017. **8**(1): p. 218.
579 29. Förster, A., et al., *Beyond Pathogenic RUNX1 Germline Variants: The Spectrum of Somatic*
580 *Alterations in RUNX1-Familial Platelet Disorder with Predisposition to Hematologic*
581 *Malignancies.* Cancers (Basel), 2022. **14**(14).
582 30. Labuhn, M., et al., *Mechanisms of Progression of Myeloid Preleukemia to Transformed Myeloid*
583 *Leukemia in Children with Down Syndrome.* Cancer Cell, 2019. **36**(2): p. 123-138.e10.
584 31. Grimm, J., D. Heckl, and J.H. Klusmann, *Molecular Mechanisms of the Genetic Predisposition*
585 *to Acute Megakaryoblastic Leukemia in Infants With Down Syndrome.* Front Oncol, 2021. **11**:
586 p. 636633.
587 32. Gialesaki, S., et al., *RUNX1 isoform disequilibrium promotes the development of trisomy 21–*
588 *associated myeloid leukemia.* Blood, 2023. **141**(10): p. 1105-1118.
589 33. Vader, G., *Pch2TRIP13: controlling cell division through regulation of HORMA domains.*
590 Chromosoma, 2015. **124**(3): p. 333-339.
591 34. Subramanian, A., et al., *Gene set enrichment analysis: A knowledge-based approach for*
592 *interpreting genome-wide expression profiles.* Proceedings of the National Academy of
593 Sciences, 2005. **102**(43): p. 15545-15550.
594 35. Banerjee, R., et al., *TRIP13 promotes error-prone nonhomologous end joining and induces*
595 *chemoresistance in head and neck cancer.* Nat Commun, 2014. **5**: p. 4527.
596 36. Jeong, H., et al., *TRIP13 Participates in Immediate-Early Sensing of DNA Strand Breaks and ATM*
597 *Signaling Amplification through MRE11.* Cells, 2022. **11**(24).
598 37. Sullivan, K.D., et al., *Mechanisms of transcriptional regulation by p53.* Cell Death &
599 Differentiation, 2018. **25**(1): p. 133-143.
600 38. Kruse, J.-P. and W. Gu, *Modes of p53 Regulation.* Cell, 2009. **137**(4): p. 609-622.
601 39. Andrysik, Z., et al., *PPM1D suppresses p53-dependent transactivation and cell death by*
602 *inhibiting the Integrated Stress Response.* Nat Commun, 2022. **13**(1): p. 7400.
603 40. Wang, Y., et al., *A Small-Molecule Inhibitor Targeting TRIP13 Suppresses Multiple Myeloma*
604 *Progression.* Cancer Res, 2020. **80**(3): p. 536-548.
605 41. Agarwal, S., et al., *DCZ0415, a small-molecule inhibitor targeting TRIP13, inhibits EMT and*
606 *metastasis via inactivation of the FGFR4/STAT3 axis and the Wnt/β-catenin pathway in*
607 *colorectal cancer.* Mol Oncol, 2022. **16**(8): p. 1728-1745.
608 42. Dong, S., et al., *Design and synthesis of cantharidin derivative DCZ5418 as a TRIP13 inhibitor*
609 *with anti-multiple myeloma activity in vitro and in vivo.* Bioorg Med Chem Lett, 2024. **98**: p.
610 129590.
611 43. Konopleva, M., et al., *MDM2 inhibition: an important step forward in cancer therapy.*
612 Leukemia, 2020. **34**(11): p. 2858-2874.
613 44. Afreen, S., et al., *BCL-XL expression is essential for human erythropoiesis and engraftment of*
614 *hematopoietic stem cells.* Cell Death Dis, 2020. **11**(1): p. 8.
615 45. Pullarkat, V.A., et al., *Venetoclax and Navitoclax in Combination with Chemotherapy in Patients*
616 *with Relapsed or Refractory Acute Lymphoblastic Leukemia and Lymphoblastic Lymphoma.*
617 Cancer Discov, 2021. **11**(6): p. 1440-1453.

46. Straube, J., S.W. Lane, and T. Vu, *Optimizing DNA hypomethylating therapy in acute myeloid leukemia and myelodysplastic syndromes.* Bioessays, 2021. **43**(10): p. e2100125.
47. Maslah, N., et al., *Niclosamide combined to Azacitidine to target TP53-mutated MDS/AML cells.* Leukemia, 2024. **38**(7): p. 1630-1633.
48. DiNardo, C.D., et al., *Phase 1 dose escalation study of the MDM2 inhibitor milademetan as monotherapy and in combination with azacitidine in patients with myeloid malignancies.* Cancer Med, 2024. **13**(14): p. e70028.
49. Cazzola, A., et al., *Prenatal Origin of Pediatric Leukemia: Lessons From Hematopoietic Development.* Front Cell Dev Biol, 2020. **8**: p. 618164.
50. Rettinger, E., et al., *The hallmarks of hematopoietic stem cell transplantation for pediatric acute myeloid leukemia.* Leukemia, 2025.
51. Heikamp, E.B., et al., *The menin-MLL1 interaction is a molecular dependency in NUP98-rearranged AML.* Blood, 2022. **139**(6): p. 894-906.
52. Troester, S., et al., *Transcriptional and epigenetic rewiring by the NUP98::KDM5A fusion oncoprotein directly activates CDK12.* Nat Commun, 2025. **16**(1): p. 4656.
53. Ogasawara, S., et al., *Novel inhibitors targeting PPM1D phosphatase potently suppress cancer cell proliferation.* Bioorg Med Chem, 2015. **23**(19): p. 6246-9.
54. Mapelli, M. and A. Musacchio, *MAD contortions: conformational dimerization boosts spindle checkpoint signaling.* Curr Opin Struct Biol, 2007. **17**(6): p. 716-25.
55. Schmoellerl, J., et al., *CDK6 is an essential direct target of NUP98 fusion proteins in acute myeloid leukemia.* Blood, 2020. **136**(4): p. 387-400.
56. Shimura, T., et al., *Cyclin D1 overexpression perturbs DNA replication and induces replication-associated DNA double-strand breaks in acquired radioresistant cells.* Cell Cycle, 2013. **12**(5): p. 773-82.
57. Domingo-Reinés, J., et al., *The pediatric leukemia oncoprotein NUP98-KDM5A induces genomic instability that may facilitate malignant transformation.* Cell Death Dis, 2023. **14**(6): p. 357.
58. Bell, H.L., et al., *Combination p53 activation and BCL-xL/BCL-2 inhibition as a therapeutic strategy in high-risk and relapsed acute lymphoblastic leukemia.* Leukemia, 2024. **38**(6): p. 1223-1235.
59. Gress, V., et al., *CBFA2T3::GLIS2 pediatric acute megakaryoblastic leukemia is sensitive to BCL-XL inhibition by navitoclax and DT2216.* Blood Adv, 2024. **8**(1): p. 112-129.
60. Nechiporuk, T., et al., *The TP53 Apoptotic Network Is a Primary Mediator of Resistance to BCL2 Inhibition in AML Cells.* Cancer Discov, 2019. **9**(7): p. 910-925.
61. Pan, R., et al., *Synthetic Lethality of Combined Bcl-2 Inhibition and p53 Activation in AML: Mechanisms and Superior Antileukemic Efficacy.* Cancer Cell, 2017. **32**(6): p. 748-760.e6.
62. Kiziltepe, T., et al., *5-Azacytidine, a DNA methyltransferase inhibitor, induces ATR-mediated DNA double-strand break responses, apoptosis, and synergistic cytotoxicity with doxorubicin and bortezomib against multiple myeloma cells.* Mol Cancer Ther, 2007. **6**(6): p. 1718-27.
63. Conneely, S.E. and A.M. Stevens, *Acute Myeloid Leukemia in Children: Emerging Paradigms in Genetics and New Approaches to Therapy.* Curr Oncol Rep, 2021. **23**(2): p. 16.

Contributions

L.N.C performed experiments, analyzed and interpreted the data, and wrote the manuscript; L.P., H.I., and C.I. performed experiments, analyzed the data, and revised the manuscript; K.S. performed bioinformatics analysis and revised the manuscript; K.M., and L.G. performed experiments; M.V. revised the manuscript; A.S. supervised

664 the analyses and revised the manuscript; J.-H.K. and D.H. designed the study,
665 analyzed and interpreted the data, wrote the manuscript, and academically drove the
666 project.

667 Acknowledgments

668 The authors thank D. Trono of EPFL (Lausanne, Switzerland), for kindly providing both
669 pMD2.G (plasmid 12259; Addgene) and psPAX2 (plasmid 12260; Addgene); A. Santos
670 (University of Halle-Wittenberg) for assistance with flow cytometry; and K. Huke for
671 assistance with animal experiments.

672 L.N.C, M.V., and D.H. were supported by the Frankfurt Foundation for Children with
673 Cancer. This work was supported by the German José Carreras Leukemia Foundation
674 (DJCLS 12 R/2024) and by grants from the parents´ Association "Hilfe für Krebskranke
675 Kinder e.V." (L.N.C, J.-H.K. and D.H).

676 Illustrations (Figures 1a, 2a, 4a and 5d and graphical abstract;
677 https://BioRender.com/3to2ktx, https://BioRender.com/q0hsqlg,

678 https://BioRender.com/qo23x2o, https://BioRender.com/3q2on7c,
679 https://biorender.com/94pt6jg) were created in BioRender.com.